Research Article

Received: 15 February 2020 Revised: 15 March 2020 Accepted article published: 28 March 2020 Published online in Wiley Online Library: 24 April 2020

(wileyonlinelibrary.com) DOI 10.1002/pi.6009

Self-assembled nanostructures of diblock copolymer films under homopolymer topcoats

Siyu Ji, Runrong Zhang, Liangshun Zhang,* Yuan Yuan and Jiaping Lin*

Abstract

To mitigate the interface energies of block copolymers with high interaction parameters, a topcoat strategy has been experimentally proposed to produce perpendicular oriented domains on a length scale of sub-10 nm. However, the origin of perpendicular oriented domains and the effect of topcoats on the self-assembled nanostructures remain to be uncovered. Herein, we use the dynamic self-consistent field theory to explore the self-assembly behaviors of symmetric block copolymer films under homopolymer topcoats. It is clearly demonstrated that the introduction of homopolymer topcoats enables a wide formation range of perpendicular oriented lamellae, originating from the fluctuating diblock copolymer/homopolymer interfaces in the process of in-plane microphase separation of block copolymer films. Our simulation results also demonstrate that the formation range of perpendicular oriented lamellae can be tuned by changing the wetting properties of homopolymer topcoats and the thickness of block copolymer films, but is weakly dependent upon the chain length of homopolymers. Our theoretical findings have wide implications for understanding the formation of perpendicular oriented domains of block copolymer films, which are important for the rational design of self-assembled nanostructures with new horizons for block copolymer lithography.

Keywords: diblock copolymers; self-consistent field theory; topcoating; directed self-assembly; self-assembled nanostructures

INTRODUCTION

Over the past decade, thin films of block copolymers have attracted considerable interest in the semiconductor industry because of their ability to self-assemble into periodic nanostructures,[1–6] which are promising for integration into the next-generation lithography technologies. Such technologies require effective control over the formation of perpendicular oriented domains for the purpose of achieving high-aspect-ratio images in pattern transfer steps. In diblock copolymer films, the orientation of self-assembled nanostructures is primarily influenced by the surface energies at the respective interfaces and the film thickness relative to the natural periodicity. Especially, theory and experiments have demonstrated that the perpendicular orientation of self-assembled nanostructures becomes favorable when the diblock copolymers are confined between two neutral surfaces.[7–13] In order to achieve the sub-10 nm technological node in the semiconductor industry, diblock copolymer films with high Flory–Huggins interaction parameters of distinct blocks should be used in the process of directed self-assembly.[14–18] However, for most diblock copolymers, the constituent blocks have considerably dissimilar surface energies, which impede the achievement of perpendicular domains throughout the thin films.

This challenge can be circumvented by the use of topcoat layers to achieve similar surface energies.[19–26] As a typical example, Willson and co-workers proposed reactive homopolymer topcoats to mitigate the surface energies through spin-coating from solution and then washing away after self-assembly.[19] Such nonpreferential or weakly preferential surfaces have been shown to produce perpendicular domains throughout films. In other work, Nealey's group combined lithographically defined substrates with topcoats to direct the self-assembly of block copolymers.[25] The topcoats are composed of homopolymers with preferential wetting towards one of the blocks or random copolymers with nonpreferential wetting towards the template-guided copolymers. It was experimentally revealed that perpendicular nanostructures are found for the nonpreferential wetting topcoats, whereas mixed perpendicular and parallel oriented nanostructures are observed for the preferential wetting topcoats. In comparison with diblock copolymers confined between hard surfaces, one of the important distinctions is that diblock copolymer films under polymer topcoats can adjust locally their height.[27–33] Consequently, novel self-assembled nanostructures and self-assembly behaviors can emerge that are not identified in systems of diblock copolymers confined between two hard walls. However, it is still difficult to directly visualize the inner component and morphological evolution of self-assembled nanostructures in experiments, which hinders the rational construction of perpendicular domains for lithographic applications.

Computational modeling provides direct information of self-assembled nanostructures throughout the polymer films and thereby complements and strengthens experimental observations.[34–36] Currently, theoretical studies of diblock copolymer films under polymer

* *Correspondence to: L Zhang or J Lin, Shanghai Key Laboratory of Advanced Polymeric Materials, Key Laboratory for Ultrafine Materials of Ministry of Education, School of Materials Science and Engineering, East China University of Science and Technology, Shanghai 200237, China. E-mail: zhangls@ecust.edu.cn (Zhang); jlin@ecust.edu.cn (Lin)*

Shanghai Key Laboratory of Advanced Polymeric Materials, Key Laboratory for Ultrafine Materials of Ministry of Education, School of Materials Science and Engineering, East China University of Science and Technology, Shanghai, China

topcoats are limited and focus on the simulations of equilibrium nanostructures.[10,21,37] For instance, on the basis of modified self-consistent field theory, a coarse-grained model was developed to probe the self-assembled nanostructures of diblock copolymers under homopolymer topcoats.[37] By searching in the parameter spaces of polymeric materials, the conditions of achieving the perpendicular domains are identified in a much wider range. Nevertheless, the fundamental principles of self-assembly behaviors, that is, the origin of perpendicular domains forming in a wide range and the effect of homopolymer topcoats on the morphological evolution, remain to be uncovered.

The aim of the work reported here was to investigate the complex and interesting self-assembly behaviors of diblock copolymer films under homopolymer topcoats. More specifically, using the dynamic self-consistent field theory (DSCFT),[38–40] we address the effect of homopolymer topcoats on the formation of self-assembled nanostructures of symmetric diblock copolymers. From the morphological evolution of self-assembled nanostructures, we find a wide formation range of perpendicular oriented domains originating from the fluctuating interfaces in the process of in-plane microphase separation, which are strongly dependent upon the wetting properties of the homopolymers and the thickness of the diblock copolymer films.

MODEL AND METHODS

In the experiments, the topcoat layers are composed of homopolymers or random copolymers to weaken the preferential wetting towards the diblock copolymers.[19,25] An advantage of this strategy is that the topcoats can be easily removed after the self-assembly of the diblock copolymers, because the macrophase-separated state of diblock copolymer/homopolymer mixtures can be preserved. In order to model such an experimental system, we consider a homopolymer topcoat placed on top of a diblock copolymer film, which is schematically illustrated in Fig. 1.

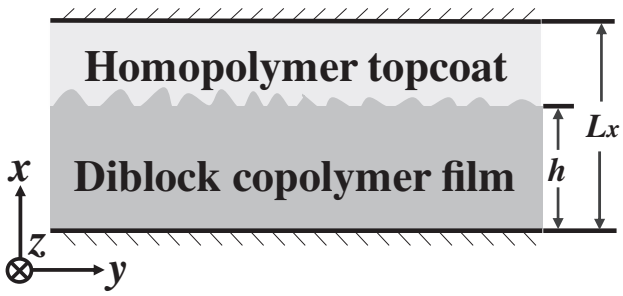

Figure 1. Schematic illustration of the self-assembly system considered. Diblock copolymer films under homopolymer topcoats are confined between two hard walls. Note that the top wall is used to model the free surface with homopolymers exposed to air in experiments. The thickness of diblock copolymers is denoted by h. The total thickness of diblock copolymer/homopolymer mixtures is represented by L_x.

The system considered here contains n_D and n_H monodisperse AB diblock copolymers and homopolymers (designated as H) in a volume V, which are confined between two impenetrable hard walls (W). The field-theoretic equations of the confined system are constructed using the standard Gaussian-chain model with the Flory–Huggins-type interaction parameters χ_{IJ}, which describe the strength of interactions between dissimilar I- and J-type beads (I and J = A, B, H and W). The chain lengths of AB diblock copolymer and homopolymer are denoted by N and $N_H = \alpha N$ beads, respectively. The volume fraction of A blocks in the diblock copolymers is represented by f. The volume fraction of diblock copolymers in the system is given by c. The free energy functional F (in units of thermal energy k_BT) per chain is written as[41]

$$F=\frac{1}{V}\int d\mathbf{r}\left\{\frac{1}{2}\sum_{I\neq J}\chi_{IJ}N\varphi_I\varphi_J-\sum_I\omega_I\varphi_I+\sum_I\chi_{IW}^{t(b)}N\varphi_I\varphi_W+\frac{\kappa}{2}\left(\sum_I\varphi_I-1\right)^2\right\}-c\ln Q_{AB}-\frac{1-c}{\alpha}\ln Q_H \quad (1)$$

where $Q_{AB(H)}$ represents the normalized single-chain partition function for the diblock copolymers (homopolymers). The external potential fields ω_I acting on the diblock copolymers are bijectively related to the given density fields by the density functional $\varphi_I[\omega_I]$. κ is the Helfand-type coefficient, which assigns a finite compressibility to the system. The third term on the right-hand side of Eqn (1) represents the contribution of walls via a short-range potential field φ_W. The magnitude $\chi_{IW}^{t(b)}$ indicates the strength of interactions between the I-type beads and the top (bottom) walls.

The structural evolution of the multicomponent system is described by the Cahn–Hilliard–Cook equations,[38,42–45] where the density fields $\varphi_I(\mathbf{r}, t)$ at position $\mathbf{r}$ and time t are chosen as order parameters. The set of quantities obey the following diffusion equation:

$$\frac{\partial\varphi_I(\mathbf{r},t)}{\partial t}=M_I\nabla\cdot\varphi_I(\mathbf{r},t)\nabla\mu_I(\mathbf{r})+\eta_I(\mathbf{r},t) \quad (2)$$

where M_I are the mobility coefficients of I-type blocks. The intrinsic chemical potentials μ_I are calculated from the functional derivative $\mu_I(\mathbf{r}) \equiv \delta F[\varphi_I]/\delta\varphi_I$. η_I are the Gaussian thermal noises satisfying the fluctuation-dissipation relationship.

In order to mimic the experimental setup, the initial state of DSCFT simulations consists of two domains: one is the homopolymer-rich domain in the upper region of the simulation boxes, and the other is the domain of uniformly distributed diblock copolymers close to the bottom wall.[27] The diblock copolymers are assumed to be symmetric and the Flory–Huggins interaction parameter $\chi_{AB}N$ is fixed at 20.0. The Helfand-type coefficient κ has a value of 200. For these choices of parameters, the natural periodicity of lamellae is determined as $L_0 \sim 4.0R_g$ (where R_g is the ideal gyration radius of diblock copolymer chains). The total thickness L_x of diblock copolymer film and homopolymer topcoat is set as $6.0R_g$. The thickness of diblock copolymer film is set as $h = 2L_x/3 = 4.0R_g$, which is commensurate with the natural periodicity of lamellae. The top wall exhibits a preference for the homopolymer topcoat ($\chi_{AW}^{t}N=\chi_{BW}^{t}N=2.0$ and $\chi_{HW}^{t}N=0.0$). The bottom wall is neutral with the diblock copolymers ($\chi_{AW}^{b}N=\chi_{BW}^{b}N=0.0$ and $\chi_{HW}^{b}N=2.0$). The use of this initial

state and the settings of interaction parameters facilitate the formation of a macrophase-separated state.

We perform the numerical simulations in three-dimensional boxes under the no-flux boundary condition in the x direction and the periodic boundary conditions in the y and z directions. In order to ensure the simulation boxes are large enough, the dimensions of boxes in the y and z directions are set as *ca* $48.0R_g \times 48.0R_g$, which are discretized by 192×192 lattices. The dimension of boxes in the x direction is discretized by 48 lattices. The discrete time in Eqn (2) is set as $\Delta t = 0.1\tau$, where τ is the time unit in the simulations. To accomplish the computational task, the GPGPU (General-Purpose Graphics Processing Unit) using NVIDIA® CUDA™ architecture is adopted to accelerate the numerical calculations of DSCFT equations of polymeric fluids.[46]

RESULTS AND DISCUSSION

Previous works have demonstrated that the incorporation of homopolymers plays an important role in determining the microphase separation of diblock copolymers.[47,48] However, a distinct feature of the self-assembly of diblock copolymer films under homopolymer topcoats is the existence of incompatible diblock copolymer/homopolymer interfaces to expand the formation range of perpendicular oriented domains for lithographic patterning applications. Below, using the DSCFT simulations, we go beyond past studies and carry out a kinetic study of the self-assembly of diblock copolymer films under the homopolymer topcoats, which are confined between hard walls. We examine the effects of material characteristics including the degree of incompatibility, the chain length and the film thickness, and delineate the conditions for the perpendicular oriented domains.

In the topcoat strategy, homopolymers are placed on top of diblock copolymer films. The preference of diblock copolymers is described by the combined Flory–Huggins interaction parameters $\chi_{IH}N$ instead of $\chi_{IW}N$. The initial thickness of diblock copolymer films is set as the commensurate value $h = L_0 = 4.0R_g$. To balance the mixing entropy gain of homopolymer chains and the computational cost, the chain length of homopolymers is chosen as $N_H = 0.3N$. Figure 2(a) illustrates the self-assembled nanostructures of diblock copolymers under the homopolymer topcoats. The DSCFT simulations are performed in the large-cell simulation boxes, but only a portion of the boxes are shown for clarity. The insets depict the averaged density distributions of diblock copolymers and homopolymers along the x direction. The average density is defined as $\bar{\varphi}_I(x) = \sum_{y,z}\varphi_I(x,y,z)/N_yN_z$, where N_y and N_z are, respectively, the lattice numbers in the y and z directions. By changing the interaction parameters between the diblock copolymers and the homopolymers, a set of self-assembled nanostructures are identified and classified into four categories: perpendicular oriented lamellae ($L_\perp$), parallel oriented lamellae ($L_\parallel$), nonbulk nanostructures (L_n, combination of perforated layers and perpendicular lamellae) and dissolved nanostructures (L_d, penetration of homopolymers into diblock copolymer films).

Figure 2(b) summarizes the self-assembled nanostructures of diblock copolymer films under the homopolymer topcoats in terms of the interaction parameters $\chi_{IH}N/\chi_{AB}N$ between the I-type blocks and homopolymers. In general, the self-assembled nanopatterns obtained from the large-cell simulations of DSCFT consist of many defective nanostructures in spite of the long-time calculations. Such kinetically trapped states plotted in Fig. 2(b) are the long-lived nanopatterns in the large-cell DSCFT simulations. Note

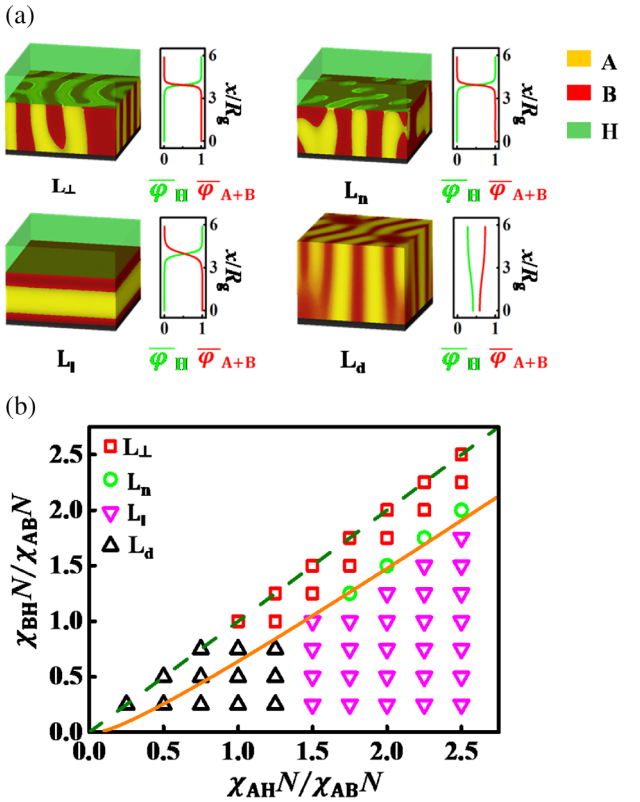

Figure 2. (a) Self-assembled nanostructures of diblock copolymer films under homopolymer topcoats: perpendicular lamellae ($L_\perp$), nonbulk structures (L_n), parallel lamellae ($L_\parallel$) and dissolved structures (L_d). The A-/B-/H-rich domains and bottom walls are represented by the yellow/red/green and black colors, respectively. Only 1/9 portion of large-cell simulation boxes is shown. Insets display the averaged densities of diblock copolymers ($\bar{\varphi}_{A+B}$) and homopolymers ($\bar{\varphi}_H$) along the x direction. (b) Long-lived nanostructures of diblock copolymer films with respect to the Flory–Huggins interaction parameters $\chi_{AH}N/\chi_{AB}N$ and $\chi_{BH}N/\chi_{AB}N$. Each point corresponds to a simulation result. The solid line represents the predicted boundary of Eqn (5) with the fitting parameters $\sigma = 1.0$ and $\delta = 0.2$. The dashed line corresponds to the case of $\sigma = 1.0$ and $\delta = 0$.

that the diagram is symmetric with respect to the dashed line $\chi_{AH}N/\chi_{AB}N = \chi_{BH}N/\chi_{AB}N$ and only the lower panel is plotted. Around the dashed line, the diblock copolymer films self-assemble into perpendicular oriented lamellae, because the interfacial energy between the homopolymers and each block is similar. Deviation from the dashed line implies the case of asymmetric interactions, leading to the preferential wetting of one of the blocks. The nanostructures transit from perpendicular oriented lamellae to nonbulk nanostructures, which are the combination of perforated layers at the diblock copolymer/homopolymer interfaces with the perpendicular lamellae emerging from the bottom walls. Moving further away from the dashed line, parallel oriented lamellae are observed owing to the strongly preferential wetting of the blocks. From the density distributions in the $L_\perp$, L_n and $L_\parallel$ nanostructures (insets of Fig. 2(a)), the homopolymers are excluded from the diblock copolymer films due to their strong incompatibility. However, in the case of weak incompatibility, the homopolymers mix with one or both of the blocks, thereby considerably altering the internal structures. Because of the penetration of homopolymers into the diblock copolymer films, such dissolved nanostructures not discussed below will lead to difficulty in the removal of homopolymer topcoats for lithographic

applications. It should be pointed out that the topcoat strategy can be integrated with directed self-assembly (e.g. utilization of chemical or topographical templates) to achieve defect-free lamellae with perpendicular orientation.[25]

In the diblock copolymers confined between the commensurate hard walls, perpendicular oriented lamellae are formed under the condition of $\chi_{AH}N/\chi_{AB}N = \chi_{BH}N/\chi_{AB}N$ (highlighted by the dashed line in Fig. 2(b)). The introduction of homopolymer topcoats expands the formation range of perpendicular oriented lamellae (solid line in Fig. 2(b)) and even changes the self-assembled nanostructures of diblock copolymer films (e.g. nonbulk and dissolved nanostructures shown in Fig. 2(a)).[37] To understand the intriguing behaviors of multicomponent systems, we further probe the morphological evolution of self-assembled nanostructures of diblock copolymer films, which is difficult to resolve from experimental observations and equilibrium simulations.

Figures 3–6 depict the morphological evolution of self-assembled nanostructures of diblock copolymer films under the homopolymer topcoats for given Flory–Huggins interaction parameters. For clarity, we only show the self-assembled nanostructures below the diblock copolymer/homopolymer interfaces defined as $\varphi_A + \varphi_B = \varphi_H$ along the x direction, which are shown in panel (a) of each figure. Correspondingly, the density field $\varphi_{A,i}(y, z)$ and the film height $h_i(y, z)$ of diblock copolymers at the interfaces are plotted in panels (b) and (c), respectively, of each figure. It should be pointed out that the film height of diblock copolymers at the interfaces is slightly larger than the setting value $h = 4.0R_g$ due to our artificial definition of diblock copolymer/homopolymer interfaces.

When the homopolymer topcoats are neutral (Fig. 3), small domains are initially formed in the diblock copolymer films ($t = 30\tau$). The domains mutually coalesce into the larger grains of perpendicular oriented lamellae with a large number of defects ($t = 150\tau$ and 1000τ). Although the structural evolution is similar to the case of symmetric diblock copolymers confined between hard walls,[49] there are some salient features of microphase separation of diblock copolymer films under the homopolymer topcoats. In the layer close to the interface, there is some moderate microphase separation causing small variation in film height $h_i(y, z)$, as illustrated in Figs 3(b) and (c). As the assembly time progresses, the interfaces can adapt their shape to the energetically and entropically most preferred structures. As a result, the diblock copolymer films show a local height modulation. Finally, the diblock copolymer films self-assemble into perpendicular oriented lamellae with the fluctuations of film height at the assembly time $t = 10\,000\tau$.

As the interaction parameters become asymmetric (e.g. $\chi_{AH}N/\chi_{AB}N = 2.00$ and $\chi_{BH}N/\chi_{AB}N = 1.75$), a different scenario of morphological evolution is identified in Fig. 4. The diblock copolymer films initially undergo vertical stratification to form a flat, homogenous B-rich layer ($t = 30\tau$), due to the preferential attractions between the B blocks and the homopolymers. Then, this flat layer begins to break up (e.g. $t = 150\tau$ and 1000τ), implying the occurrence of in-plane microphase separation at the interfaces.[50,51] Concurrently, the diblock copolymers self-assemble into small domains in the inner films. The fluctuation amplitude of film height becomes large. With an increase of the simulation time, the perpendicular oriented lamellae are finally achieved and the diblock copolymer/homopolymer interfaces become rough.

When the asymmetry of interaction parameters is further increased, the break-up of flat B-rich layers is observed in the initial stage due to the in-plane microphase separation (Fig. 5; parameter settings of $\chi_{AH}N/\chi_{AB}N = 2.00$ and $\chi_{BH}N/\chi_{AB}N = 1.50$). However, the coupled roughening is more marked in comparison with the case of Fig. 4. In particular, due to the higher selectivity of homopolymer topcoats, the B-rich domains are more dominant than the A-rich domains at the interfaces. With an increase of the simulation time, the short A-rich domains coalesce into long ones dispersed in the continuous B-rich domains at the interfaces.

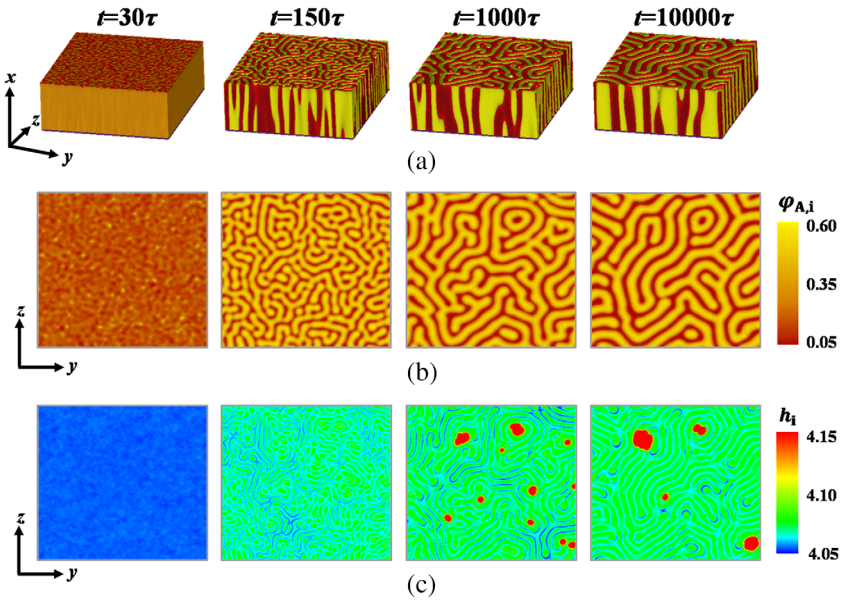

Figure 3. (a) Morphological evolution of perpendicular lamellar nanostructures of diblock copolymer film under homopolymer topcoat. The Flory–Huggins interaction parameters are set as $\chi_{AH}N/\chi_{AB}N = 2.00$ and $\chi_{BH}N/\chi_{AB}N = 2.00$. Only the A- and B-rich domains are shown in the snapshots. (b) Top-down view of density field distribution of A blocks at the diblock copolymer/homopolymer interface. (c) Top-down view of film height of diblock copolymers at the interface.

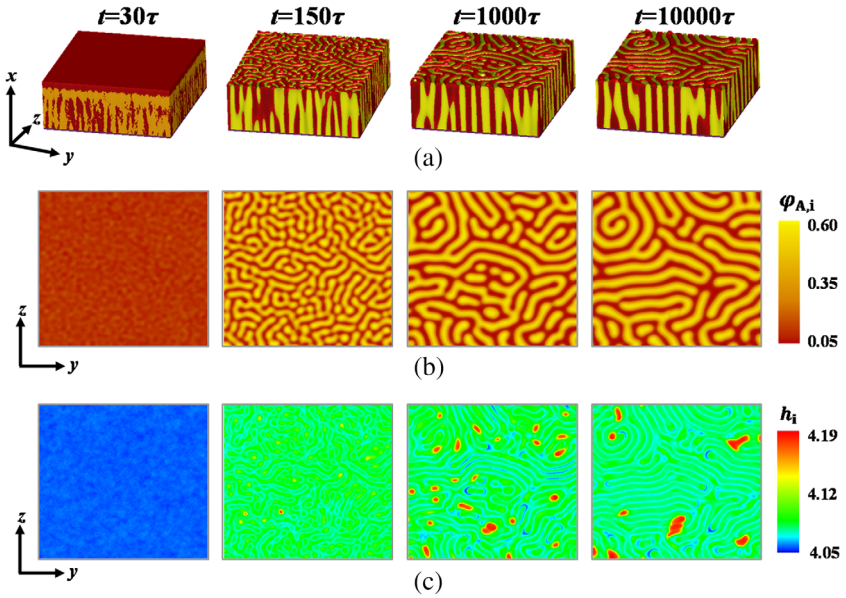

Figure 4. (a) Morphological evolution of perpendicular lamellar nanostructures of diblock copolymer film under homopolymer topcoat. The Flory–Huggins interaction parameters are set as $\chi_{AH}N/\chi_{AB}N = 2.00$ and $\chi_{BH}N/\chi_{AB}N = 1.75$. (b) Top-down view of density field distribution of A blocks at the diblock copolymer/homopolymer interface. (c) Top-down view of film height of diblock copolymers at the interface.

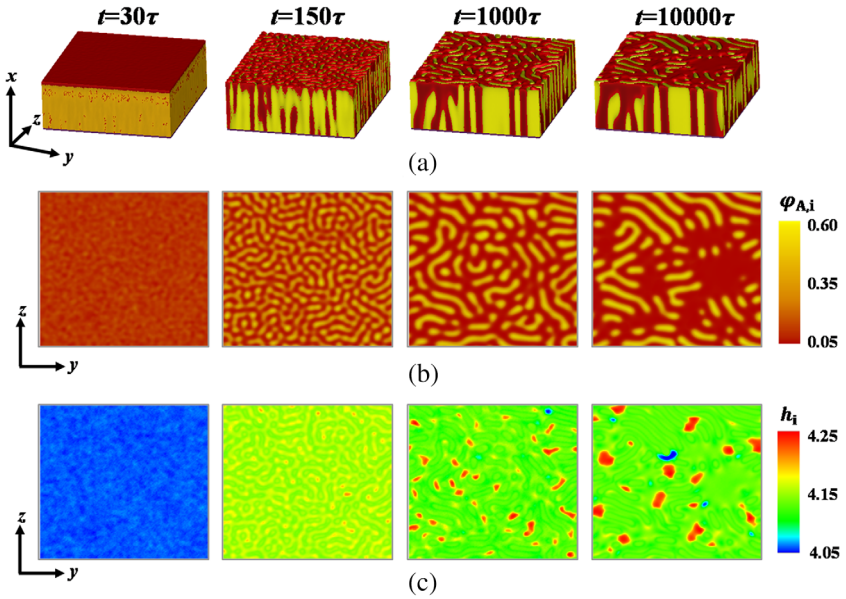

Figure 5. (a) Morphological evolution of nonbulk nanostructures of diblock copolymer film under homopolymer topcoat. The Flory–Huggins interaction parameters are set as $\chi_{AH}N/\chi_{AB}N = 2.00$ and $\chi_{BH}N/\chi_{AB}N = 1.50$. (b) Top-down view of density field distribution of A blocks at the diblock copolymer/homopolymer interface. (c) Top-down view of film height of diblock copolymers at the interface.

As a result, the diblock copolymer films self-assemble into nonbulk nanostructures with larger fluctuations of film height, which are the combination of perforated layers at the interfaces with the perpendicular lamellae emerging from the bottom walls.

The extreme asymmetry of interaction parameters (Fig. 6; parameter settings of $\chi_{AH}N/\chi_{AB}N = 2.00$ and $\chi_{BH}N/\chi_{AB}N = 0.50$) results in the formation of B-rich layer near the interfaces due to the strong selectivity of homopolymer topcoats. However, the domains of diblock copolymers near the bottom walls retain a vertical orientation due to the neutral walls. With an increase of the simulation time, the B-rich layer serves as a template to reorganize the nanostructures and finally favors the formation of layers parallel to the walls. It should be noted that the fluctuations of film height are small in comparison with those in other nanostructures.

Below, we introduce two variables to quantify the self-assembly kinetics of diblock copolymer films under the homopolymer topcoats. One is the standard deviation of A-block density $\varphi_{A,i}$ at the interfaces S_i defined as SD $\varphi_{A,i} = \left(\frac{1}{S_i}\int_{S_i} d\mathbf{r}\left(\varphi_{A,i} - \bar{\varphi}_{A,i}\right)^2\right)^{1/2}$ ($\bar{\varphi}_{A,i}$ is the average value of $\varphi_{A,i}$ at the interfaces S_i), which gives a measure of in-plane degree of segregation of diblock copolymers. The other

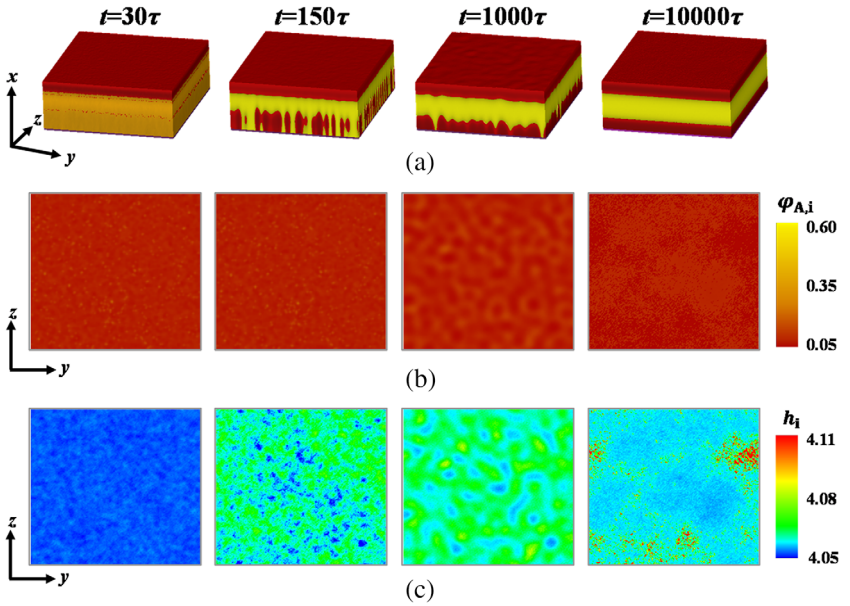

Figure 6. (a) Morphological evolution of parallel nanostructures of diblock copolymer film under homopolymer topcoat. The Flory–Huggins interaction parameters are set as $\chi_{AH}N/\chi_{AB}N = 2.00$ and $\chi_{BH}N/\chi_{AB}N = 0.50$. (b) Top-down view of density field distribution of A blocks at the diblock copolymer/homopolymer interface. (c) Top-down view of film height of block copolymers at the interface.

is the standard deviation of film height h_i defined as SD $h_i = \left(\frac{1}{S_i}\int_{S_i} d\mathbf{r}\,(h_i - \bar{h}_i)^2\right)^{1/2}$ ($\bar{h}_i$ is the average value of h_i), which gives a measure of the degree of roughness of block copolymer/homopolymer interfaces.

Figure 7 shows the standard deviation of A-block density $\varphi_{A,i}$ and film thickness h_i at the interfaces as a function of the assembly time t. In the early stage ($t < 30\tau$), the standard deviation of A-block density $\varphi_{A,i}$ at the interfaces shows a slight increase after quenching from the homogeneous states. The corresponding fluctuations of film height h_i are small. Around the time $t = 30\tau$, the in-plane microphase separation at the interfaces results in lateral inhomogeneity, corresponding to a sharp increase of SD $\varphi_{A,i}$. After the in-plane microphase separation at the interfaces (around the time $t = 150\tau$), the diblock copolymer films become rough, corresponding to a sharp increase of SD h_i. Around the time $t = 1000\tau$, the in-plane microphase separation is mostly completed and SD h_i reaches a maximum value. In the later stage, the whole nanostructures become steady and gradually adjust themselves to relax the nonflat interfaces, leading to a decrease of SD h_i. Finally, the self-assembled nanostructures contain many defects in spite of long-time simulations and SD h_i reaches a plateau value.

From Fig. 7, one can deduce an important outcome that the interaction parameter $\chi_{BH}N/\chi_{AB}N$ plays an important role in the regulation of microphase separation behaviors of diblock copolymer films. As $\chi_{BH}N/\chi_{AB}N$ is close to $\chi_{AH}N/\chi_{AB}N = 2.00$ (e.g. $\chi_{BH}N/\chi_{AB}N > 1.50$), in-plane microphase separation at the interfaces takes place, resulting in the perpendicular orientation of lamellae and the fluctuations of film height. When the interaction parameters are strongly asymmetric (e.g. $\chi_{BH}N/\chi_{AB}N = 0.50$), the wetting property of A-blocks induces the formation of flat, B-rich layers at the interfaces, where the in-plane microphase separation of block copolymers and the fluctuations of film height cannot be observed.

We also perform large-cell DSCFT simulations of diblock copolymer films ($\chi_{AH}N/\chi_{AB}N = 2.00$ and $\chi_{BH}N/\chi_{AB}N = 1.75$), whose initial configurations are the defect-free lamellae with perpendicular orientation. The dashed lines in Figs 7(a) and (b) represent the standard deviations of A-block density $\varphi_{A,i}$ and film height h_i at the interfaces, respectively. In comparison with the homogeneous initial configurations, SD h_i has a smaller value. However, the fluctuation of film height at the diblock copolymer/homopolymer interfaces is also observed in the case of defect-free lamellae. Therefore, the asymmetric interaction parameters between the diblock copolymers and homopolymers can lead to the roughness of thin films, but the long-lived defects further increase the fluctuations of film height.

As illustrated above, our simulations indicate that there are two factors for the achievement of perpendicular oriented lamellae. One is the interfacial energies of different polymers (shown in Fig. 2). The other is the roughening of free diblock copolymer/homopolymer interfaces (shown in Figs 3–7). Here, we propose a simple theoretical model considering the above factors to obtain the necessary conditions for stable lamellae with perpendicular orientation.[19,27,37] This simple model only considers the contribution of interfacial energies of different components, and neglects the contribution of chain configurations. It is assumed that the self-assembly of symmetric diblock copolymers takes place between the substrates and the homopolymer topcoats. The averaged thickness of diblock copolymer films is commensurate with the natural periodicity L_0 of lamellae, but the local height of diblock copolymer films can be adjusted. We consider a half unit cell of lateral size, i.e. $L_0/2 \times L_0$. γ_{IJ} represents a measure of the interface energies between the I- and J-type components (I and J = A, B and H). The values of γ_{IJ} are estimated using the Helfand–Tagami relation between the interfacial energies and the Flory–Huggins interaction parameters,[52] i.e. $\gamma_{IJ} \propto \sqrt{\chi_{IJ}/6}$.

Because of the narrow region of nonbulk nanostructures (Fig. 2), we only consider two candidate nanostructures of diblock copolymer films: parallel lamellae (Fig. 8(a)) and perpendicular lamellae with roughness (Fig. 8(b)). As shown in Figs 6 and 7, the fluctuations of film height for the parallel lamellae can be neglected.

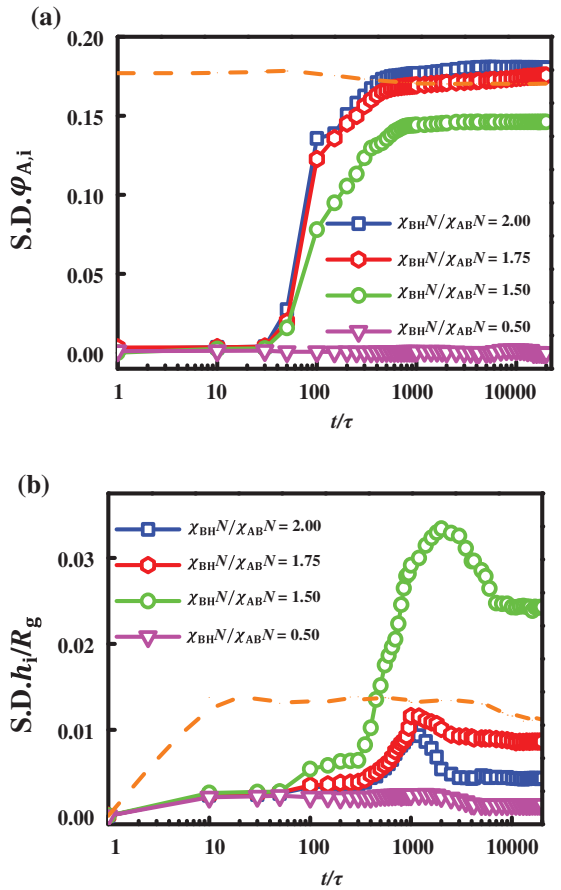

Figure 7. Standard deviation of (a) A-block density $\varphi_{A,i}$ and (b) film height h_i at the interfaces as a function of assembly time t for the diblock copolymer films under homopolymer topcoats for interaction parameters $\chi_{BH}N/\chi_{AB}N$ = 2.00, 1.75, 1.50 and 0.50. The interaction parameter $\chi_{AH}N/\chi_{AB}N$ is fixed at 2.00. In each plot, the dashed line represents the standard deviation for the large-cell simulations starting from the initial configurations of defect-free lamellae with perpendicular orientation. The parameter settings are $\chi_{AH}N/\chi_{AB}N = 2.00$ and $\chi_{BH}N/\chi_{AB}N = 1.75$.

The relative free energy of parallel lamellae (per area L_0^2) is given by

$$\Delta f_{\parallel} = \frac{1}{2}\gamma_{AH} + \gamma_{AB} \tag{3}$$

for the case of $\gamma_{BH} \le \gamma_{AH}$. For the perpendicular lamellae with roughness (Figs 3, 4 and 7), we assume that the B blocks are preferred to the homopolymer topcoats. As a result, the B-rich domains partially overlap the A-rich domains near the diblock copolymer/homopolymer interfaces, which is schematically illustrated in Fig. 8(b). The interfacial areas between different components are denoted by k_1S, k_2S and k_3S, where the prefactor k_n is used to describe the roughening of interfaces and S is the cross-section area of unit cell. The relative free energy of perpendicular lamellae with roughness is written as

$$\Delta f_{\perp} = k_1\gamma_{AH} + k_2\gamma_{BH} + k_3\gamma_{AB} \tag{4}$$

under the condition of $k_1 \le k_2$ and $k_3 \ge 1$. Note that the perfectly perpendicular lamellae correspond to the case of $k_1 = k_2 = 1/4$ and $k_3 = 1$.

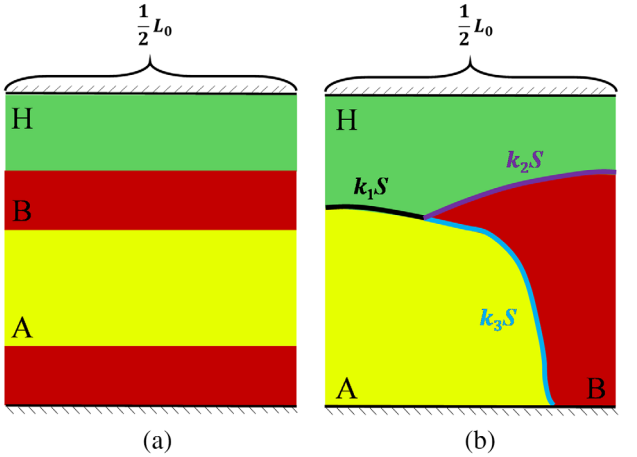

Figure 8. Schematic illustrations of (a) parallel and (b) perpendicular lamellae considered in the theoretical analysis. The A- and B-rich domains and the homopolymer topcoats are represented by the yellow, red and green colors, respectively. For the perpendicular lamellae with roughness, the interfacial areas between different components are denoted by k_1S, k_2S and k_3S.

If the perpendicular lamellae are stable, their free energy should be less than that of parallel ones. Thus, by comparing the relative free energy of perpendicular and parallel lamellae described in Eqns (3) and (4), the condition for achieving the vertical domains is written as

$$\sqrt{\frac{\chi_{AH}N}{\chi_{AB}N}} < \sigma\sqrt{\frac{\chi_{BH}N}{\chi_{AB}N}} - \delta \tag{5}$$

where $\sigma = \left(\frac{1}{2} - k_2\right)/k_1$ and $\delta = (k_3 - 1)/k_1$. This expression can be used to generate the stability boundary of self-assembled nanostructures of diblock copolymer films under the homopolymer topcoats. As shown in Fig. 2(b), the boundary of parallel lamellae and perpendicular ones with roughness is indicated by the solid line, which uses the fitting parameters $\sigma = 1.0$ and $\delta = 0.2$ of Eqn (5). In the case of perfectly perpendicular lamellae, the fitting parameters have the values of $\sigma = 1.0$ and $\delta = 0$. The boundary of parallel and perfectly perpendicular lamellae is represented by the dashed line. The theoretical analysis further demonstrates that the formation range of perpendicular lamellae can be further expanded in the system of diblock copolymer films under the homopolymer topcoats, originating from the roughness of free interfaces. It should be pointed out that our simulation findings and theoretical predictions are consistent with the results for diblock copolymers on rough substrates.[53,54]

When the diblock copolymer films are exposed to the homopolymer topcoats, their interfaces are regarded as free surfaces and the films can adjust their height locally. The behaviors of the systems not only depend on the Flory–Huggins interaction parameters of block copolymers and homopolymers, but also have a tight relation with the mismatch of natural periodicity with the thickness of diblock copolymer films. Figure 9(a) shows the effect of film thickness on the self-assembled nanostructures of diblock copolymer films under the homopolymer topcoats. As the film thickness becomes incommensurate (i.e. the value of h deviates from the natural periodicity $L_0 = 4.0R_g$), the range of $\chi_{BH}N/\chi_{AB}N$ leading to the formation of perpendicular lamellae becomes broad, implying that the properties of diblock copolymer/

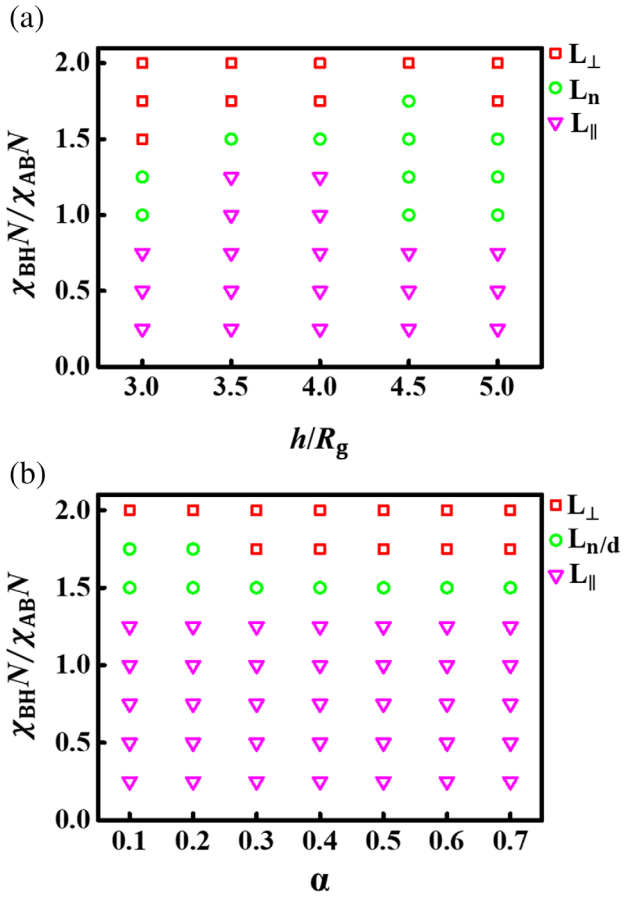

Figure 9. Effects of (a) thickness of diblock copolymer films and (b) length of homopolymer chains on the self-assembled nanostructures. The representations of symbols are the same as those of Fig. 2. In (a), the thickness ratio of diblock copolymer films and diblock copolymer/homopolymer films is fixed at $h/L_x = 2/3$. In (b), α represents the length ratio of homopolymer to diblock copolymer chains. The thickness of diblock copolymer film is chosen as $h = 4.0R_g$. The interaction parameter is set as $\chi_{AH}N/\chi_{AB}N = 2.00$.

homopolymer interfaces can be further extended away from the neutral region. It should be mentioned that the thick diblock copolymer films mainly self-assembly into the nonbulk nanostructures.

In the topcoat strategy, the chain length of homopolymers is a tunable parameter to control the self-assembly behaviors of diblock copolymer films. Figure 9(b) illustrates the effect of chain length $N_H = \alpha N$ of homopolymers on the self-assembled nanostructures of diblock copolymer films. Under the condition of $N_H \geq 0.3N$, the chain length of homopolymers has a slight effect on the formation range of perpendicular lamellae due to the weak penetration of homopolymers into the diblock copolymer films. As the homopolymer chains become short, the homopolymers penetrate into the diblock copolymer films to gain mixing entropy. As a result, the diblock copolymer films self-assemble into nonbulk or dissolved nanostructures (designated as $L_{n/d}$ in Fig. 9(b)) instead of perpendicular lamellae.

CONCLUSIONS

We extend the DSCFT to model the self-assembly behaviors of block copolymer films under homopolymer topcoats. This model enables us to capture the morphological evolution of self-assembled nanostructures. Using the large-cell simulations of this model, we corroborate the findings that perpendicular oriented lamellae are achieved by virtue of the topcoat strategy for the block copolymer films, and their formation range is exceptionally expanded in comparison with the case of block copolymers confined between hard walls. Through analyzing the morphological evolution of self-assembled nanostructures, it is found that the in-plane microphase separation of block copolymer films at the block copolymer/homopolymer interfaces induces fluctuations of film height, which result in a wide formation range of perpendicular oriented lamellae. On the basis of these findings, we further build upon a simple theoretical model to obtain the necessary conditions for self-assembled nanostructures with perpendicular orientations. The large-cell simulations also reveal the importance of parameter choices for achieving perpendicular oriented nanostructures of block copolymers.

AUTHOR INFORMATION

NOTES

The authors declare no competing financial interest.

ACKNOWLEDGEMENT

This work was supported by the National Natural Science Foundation of China (21574040 21873029 and 51833003).

REFERENCES

1 Cheng JY, Mayes AM and Ross CA, *Nat Mater* **3**:823–828 (2004).
2 Segalman RA, *Mater Sci Eng R* **48**:191–226 (2005).
3 Luo M and Epps TH, *Macromolecules* **46**:7567–7579 (2013).
4 Bates CM, Maher MJ, Janes DW, Ellison CJ and Willson CG, *Macromolecules* **47**:2–12 (2014).
5 Ji S, Wan L, Liu C-C and Nealey PF, *Prog Polym Sci* **54–55**:76–127 (2016).
6 Bates CM and Bates FS, *Macromolecules* **50**:3–22 (2017).
7 Matsen MW, *J Chem Phys* **106**:7781–7791 (1997).
8 Yang Y, Qiu F, Zhang H and Yang Y, *Polymer* **47**:2205–2216 (2006).
9 Li W, Liu M, Qiu F and Shi A-C, *J Phys Chem B* **117**:5280–5288 (2013).
10 Durand WJ, Carlson MC, Maher MJ, Blachut G, Santos LJ, Tein S *et al.*, *Macromolecules* **49**:308–316 (2016).
11 Arceo A and Green PF, *J Phys Chem B* **109**:6958–6962 (2005).
12 Epps TH, DeLongchamp DM, Fasolka MJ, Fischer DA and Jablonski EL, *Langmuir* **23**:3355–3362 (2007).
13 Jung J, Park H-W, Lee S, Lee H, Chang T, Matsunaga K *et al.*, *ACS Nano* **4**:3109–3116 (2010).
14 Sinturel C, Bates FS and Hillmyer MA, *ACS Macro Lett* **4**:1044–1050 (2015).
15 Wang J, Li L, Yang W, Yan Z, Zhou Y, Wang B *et al.*, *ACS Macro Lett* **8**:1012–1016 (2019).
16 Barreda L, Shen Z, Chen QP, Lodge TP, Siepmann JI and Hillmyer MA, *Nano Lett* **19**:4458–4462 (2019).
17 Jiang X-Q, Zhao R-Y, Chang W-Y, Yin D-X, Guo Y-C, Wang W *et al.*, *Macromolecules* **52**:5033–5041 (2019).
18 Pang Y, Jin X, Huang G, Wan L and Ji S, *Macromolecules* **52**:2987–2994 (2019).
19 Bates CM, Seshimo T, Maher MJ, Durand WJ, Cushen JD, Dean LM *et al.*, *Science* **338**:775–779 (2012).
20 Seshimo T, Bates CM, Dean LM, Cushen JD, Durand WJ, Maher MJ *et al.*, *J Photopolym Sci Technol* **25**:125–130 (2012).
21 Yoshida H, Suh HS, Ramirez-Herunandez A, Lee JI, Aida K, Wan L *et al.*, *J Photopolym Sci Technol.* **26**:55–58 (2013).
22 Jeong J, Ha JS, Lee S-S and Son JG, *Macromol Rapid Commun* **36**:1261–1266 (2015).
23 Sunday DF, Maher MJ, Tein S, Carlson MC, Ellison CJ, Willson CG *et al.*, *ACS Macro Lett* **5**:1306–1311 (2016).
24 Zhang J, Clark MB, Wu C, Li M, Trefonas P and Hustad PD, *Nano Lett* **16**:728–735 (2016).
25 Suh HS, Kim DH, Moni P, Xiong S, Ocola LE, Zaluzec NJ *et al.*, *Nat Nanotechnol* **12**:575–581 (2017).

26 Oh J, Suh HS, Ko Y, Nah Y, Lee J-C, Yeom B *et al.*, *Nat Commun* **10**:2912 (2019).
27 Morita H, Kawakatsu T and Doi M, *Macromolecules* **34**:8777–8783 (2001).
28 Knoll A, Horvat A, Lyakhova KS, Krausch G, Sevink GJA, Zvelindovsky AV *et al.*, *Phys Rev Lett* **89**:035501 (2002).
29 Lyakhova KS, Horvat A, Zvelindovsky AV and GJA S, *Langmuir* **22**: 5848–5855 (2006).
30 Horvat A, Knoll A, Krausch G, Tsarkova L, Lyakhova KS, Sevink GJA *et al.*, *Macromolecules* **40**:6930–6939 (2007).
31 Kim JU and Matsen MW, *Soft Matter* **5**:2889–2895 (2009).
32 Stasiak P, McGraw JD, Dalnoki-Veress K and Matsen MW, *Macromolecules* **45**:9531–9538 (2012).
33 Man X, Andelman D and Orland H, *Phys Rev E* **86**:010801 (2012).
34 Ginzburg VV, Weinhold JD and Trefonas P, *J Polym Sci B: Polym Phys* **53**: 90–95 (2015).
35 Li W and Müller M, *Prog Polym Sci* **54–55**:47–75 (2016).
36 Müller M, *Prog Polym Sci* **101**:101198 (2020).
37 Ramírez-Hernández A, Suh HS, Nealey PF and de Pablo JJ, *Macromolecules* **47**:3520–3527 (2014).
38 Fraaije JGEM, van Vlimmeren BAC, Maurits NM, Postma M, Evers OA, Hoffmann C *et al.*, *J Chem Phys* **106**:4260–4269 (1997).
39 Yeung C and Shi A-C, *Macromolecules* **32**:3637–3642 (1999).
40 Reister E, Müller M and Binder K, *Phys Rev E* **64**:041804 (2001).
41 Fredrickson GH, *The Equilibrium Theory of Inhomogeneous Polymers*. Oxford University Press, Oxford (2006).
42 Zhang L, Sevink A and Schmid F, *Macromolecules* **44**:9434–9447 (2011).
43 Cao X, Zhang L, Wang L and Lin J, *Soft Matter* **10**:5916–5927 (2014).
44 Cong Z, Zhang L, Wang L and Lin J, *J Chem Phys* **144**:114901 (2016).
45 Wan X, Gao T, Zhang L and Lin J, *Phys Chem Chem Phys* **19**:6707–6720 (2017).
46 Zhang L, Liu L and Lin J, *Phys Chem Chem Phys* **20**:498–508 (2018).
47 Matsen MW, *Phys Rev Lett* **74**:4225–4228 (1995).
48 Matsen MW, *Macromolecules* **28**:5765–5773 (1995).
49 Müller M, Li W, JCO R and Welling U, *J Phys Conf Ser* **640**:012010 (2015).
50 Coveney S and Clarke N, *Phys Rev Lett* **111**:125702 (2013).
51 Coveney S and Clarke N, *Phys Rev Lett* **113**:218301 (2014).
52 Helfand E and Tagami Y, *J Chem Phys* **56**:3592–3601 (1972).
53 Man X, Zhou P, Tang J, Yan D and Andelman D, *Macromolecules* **49**: 8241–8248 (2016).
54 Man X, Tang J, Zhou P, Yan D and Andelman D, *Macromolecules* **48**: 7689–7697 (2015).

